Chemistry & Biology
Brief Communication

# The CK2α/CK2β Interface of Human Protein Kinase CK2 Harbors a Binding Pocket for Small Molecules

Jennifer Raaf,[1] Elena Brunstein,[1] Olaf-Georg Issinger,[2] and Karsten Niefind[1,*]
[1]Institut für Biochemie, Universität zu Köln, Zülpicher Str. 47, D-50674 Köln, Germany
[2]Institut for Biokemi og Molekylær Biologi, Syddansk Universitet, Campusvej 55, DK-5230 Odense, Denmark
*Correspondence: karsten.niefind@uni-koeln.de
DOI 10.1016/j.chembiol.2007.12.012

## SUMMARY

**The Ser/Thr kinase CK2 (previously called casein kinase 2) is composed of two catalytic chains (CK2α) attached to a dimer of noncatalytic subunits (CK2β). CK2 is involved in suppression of apoptosis, cell survival, and tumorigenesis. To investigate these activities and possibly affect them, selective CK2 inhibitors are required. An often-used CK2 inhibitor is 5,6-dichloro-1-β-D-ribofuranosylbenzimidazole (DRB). In a complex structure with human CK2α, DRB binds to the canonical ATP cleft, but additionally it occupies an allosteric site that can be alternatively filled by glycerol. Inhibition kinetic studies corroborate the dual binding mode of the inhibitor. Structural comparisons reveal a surprising conformational plasticity of human CK2α around both DRB binding sites. After local rearrangement, the allosteric site serves as a CK2β interface. This opens the potential to construct molecules interfering with the CK2α/CK2β interaction.**

## INTRODUCTION

About 500 eukaryotic protein kinases (EPKs) are encoded in the human genome (Manning et al., 2002). As key components of signaling pathways, they are attractive as cell biological research subjects and pharmaceutical targets. Therefore, selective small-molecule EPK inhibitors are continually searched as valuable research tools and as candidates for drug development (Knight and Shokat, 2005).

Most EPK inhibitors address the canonical ATP cleft. Because of its structural similarity in all EPKs, it is difficult to obtain selectivity. Several strategies to overcome this problem exist (Knight and Shokat, 2005). (1) Type I inhibitors bind to the ATP sites of active EPKs and exploit structural differences in this region for molecular recognition. (2) Type II inhibitors address the ATP sites of inactive states that occur in the context of activity control of EPKs and are structurally more diverse than the active ones (Huse and Kuriyan, 2002). In particular, the so-called activation segment is a key control element with significant conformational plasticity. (3) Type III inhibitors form an increasing subset of EPK inhibitors that occupy allosteric sites rather than the ATP cleft (Knight and Shokat, 2005). (4) Finally, protein/protein interactions rather than active sites are novel inhibitor targets (Wells and McClendon, 2007). As the function of EPKs in general requires docking of various regulator and anchor proteins, this concept is an attractive vision for interfering with EPKs.

An important EPK subgroup is the CMGC kinases (Manning et al., 2002) with regulatory key enzymes such as the cyclin-dependent kinases or MAP kinases. A remote member of the CMGC kinases is CK2α (Niefind et al., 2007), which is the catalytic subunit of protein kinase CK2 (previously called casein kinase 2). The overexpression of CK2α is associated with lymphoma development (Seldin and Leder, 1995). Together with a noncatalytic subunit (CK2β), CK2α forms a heterotetrameric holoenzyme (Niefind et al., 2001; Figure 1). Unlike its CMGC relatives, CK2α is neither phosphorylated nor structurally variable at the activation segment. Rather, it is intramolecularly restrained to keep an active conformation (Niefind et al., 2007), both in monomeric form and within the CK2 holoenzyme. As CK2α and the CK2 holoenzyme strongly differ in their substrate specificities (Guerra and Issinger, 1999), the CK2α/CK2β interaction might be a target to affect the intracellular CK2 activity profile.

In the last several years, several type I CK2 inhibitors have been devised (see Nie et al., 2007, and references therein). All of them were either designed or subsequently structurally characterized in complex with maize CK2α. The inherent assumption of these studies—that maize and human CK2α are nearly identical at the ATP site—was challenged recently by the crystal structure of a human CK2α mutant (Yde et al., 2005) in which the interdomain hinge—a part of the ATP binding site—deviated distinctly from all known CK2α structures. This observation suggested that cocrystal structures of inhibitors with genuine human CK2α are worth being solved.

We therefore crystallized *hs*CK2α$^{1-335}$, a C-terminal deletion mutant of human CK2α that is fully active and capable of CK2 holoenzyme formation (Niefind et al., 2007), together with 5,6-dichloro-1-β-D-ribofuranosylbenzimidazole (DRB). DRB is a classical chemical probe for downgrading DNA transcription, and an old and relatively selective CK2 inhibitor (Meggio et al., 1990). Whether both phenomena are correlated is unclear. A 3D structure of DRB bound to CK2α or any other EPK is thus far not available from the Protein Data Bank (PDB).

## RESULTS AND DISCUSSION

### Dual Binding Mode of DRB at Human CK2α

We solved an *hs*CK2α$^{1-335}$/DRB complex structure at 1.56 Å resolution (Table 1). Surprisingly, two DRB molecules were found attached to the enzyme (Figure 1). One of them (DRB1) occupies

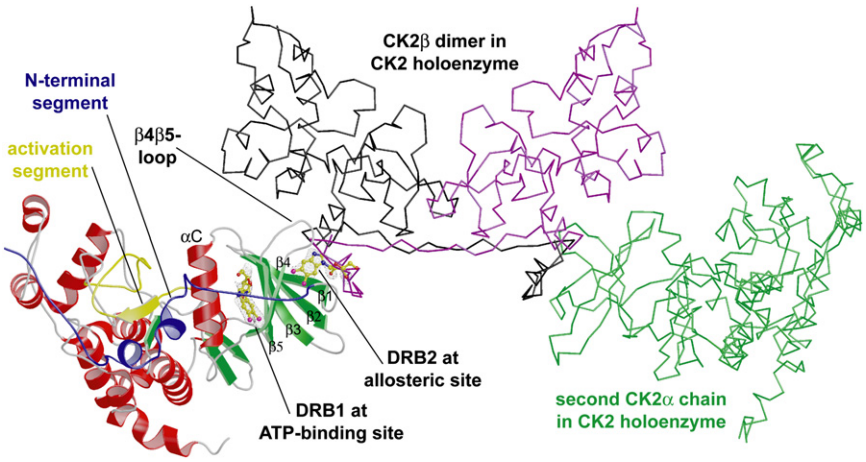


**Figure 1. Dual DRB Binding to *hs*CK2α$^{1–335}$**

The *hs*CK2α$^{1–335}$ molecule is drawn on the left-hand side. The two bound DRB molecules are covered with $F_o - F_c$ omit density (contour level 3.0 σ) calculated with the CCP4 programs (CCP4, 1994). The CK2 holoenzyme (Niefind et al., 2001) was superimposed with its first CK2α chain on the *hs*CK2α$^{1–335}$/DRB complex. Afterward, the CK2β dimer (black and purple $C_\alpha$ trace) and the second CK2α chain (green $C_\alpha$ trace) were drawn. The figure was prepared with BOBSCRIPT (Esnouf, 1997) and Raster3D (Merritt and Bacon, 1997).

the canonical ATP site (Figures 1 and 2A). The second one (DRB2) is bound to a hydrophobic pocket at the outer surface of the N-terminal β sheet (Figures 1 and 2B).

To our knowledge, such an allosteric binding site has never been reported for any inhibitor complex structure of maize CK2α (Nie et al., 2007). Therefore, we confirmed our finding

**Table 1. Data Collection and Refinement Statistics**

| | *hs*CK2α$^{1–335}$/DRB | *hs*CK2α$^{1–335}$/V66A/M163L/Glycerol[a] |
|---|---|---|
| Data Collection | | |
| Space group | $P4_32_12$ | $P4_32_12$ |
| Lattice constants *a*, *b*, *c* (Å) | 71.5, 71.5, 125.8 | 71.4, 71.4, 126.4 |
| Resolution (Å) (highest shell) | 24.8–1.56 (1.62–1.56) | 50.5–1.66 (1.71–1.66) |
| $R_{sym}$ (%) | 6.0 (60.9) | 9.9 (44.7) |
| $I/\sigma I$ | 11.7 (3.2) | 31.5 (3.2) |
| Completeness (%) | 99.9 (100.0) | 98.0 (80.1) |
| Redundancy | 7.6 (7.5) | 8.7 (5.6) |
| Refinement | | |
| Resolution (Å) | 24.8–1.56 | 50.5–1.66 |
| Number of reflections | 45,706 | 39,365 |
| $R_{work}/R_{free}$ (%) | 14.4/19.9 | 14.3/20.6 |
| Number of atoms | | |
| Protein | 2861 | 2815 |
| Ligand/ion | 56 | 38 |
| Water | 338 | 284 |
| B factors (Å$^2$) | | |
| Protein | 26.6 | 32.1 |
| Ligand/ion | 42.4 | 61.2 |
| Water | 36.4 | 44.5 |
| Root-mean-square deviations | | |
| Bond lengths (Å) | 0.017 | 0.011 |
| Bond angles (°) | 1.583 | 1.304 |

*hs*CK2α$^{1–335}$ was prepared as described by Niefind et al. (2007). The final solution contained 11.3 mg/ml *hs*CK2α$^{1–335}$ in 500 mM NaCl, 25 mM Tris/HCl (pH 8.5). A 10 mM DRB solution was prepared. One percent (v/v) dioxane and some KOH were added to improve solubility. Equal volumes of the DRB and the *hs*CK2α$^{1–335}$ stock solution were mixed and incubated at 20°C for 30 min. For crystallization with the sitting-drop method, 2 μl of the *hs*CK2α$^{1–335}$/DRB solution was mixed with 1 μl of the reservoir solution composed of 1.5 M $(NH_4)_2SO_4$, 0.2 M Na citrate, 0.2 M Na/K tartrate (pH 5.6). *hs*CK2α$^{1–335}$/DRB crystals formed at 20°C within 1 day. Cryo conditions were adjusted by replacing the reservoir solution by a 3.9 M $(NH_4)_2SO_4$ solution and subsequent equilibration. X-ray diffraction data were collected at beamline X12 of the EMBL outstation in Hamburg. The wavelength was 0.9 Å and the temperature was 100K. The diffraction data were processed with the HKL package (Otwinowski and Minor, 1997). The structure was determined by molecular replacement using MOLREP and refined with REFMAC from CCP4 (1994). For the *hs*CK2α$^{1–335}$/V66A/M163L/glycerol structure, the coordinates and structure factors of PDB ID code 1YMI (Yde et al., 2005) were downloaded. After addition of glycerol, the structure was refined with REFMAC.

[a] Diffraction data set characteristics were adopted from Yde et al. (2005).

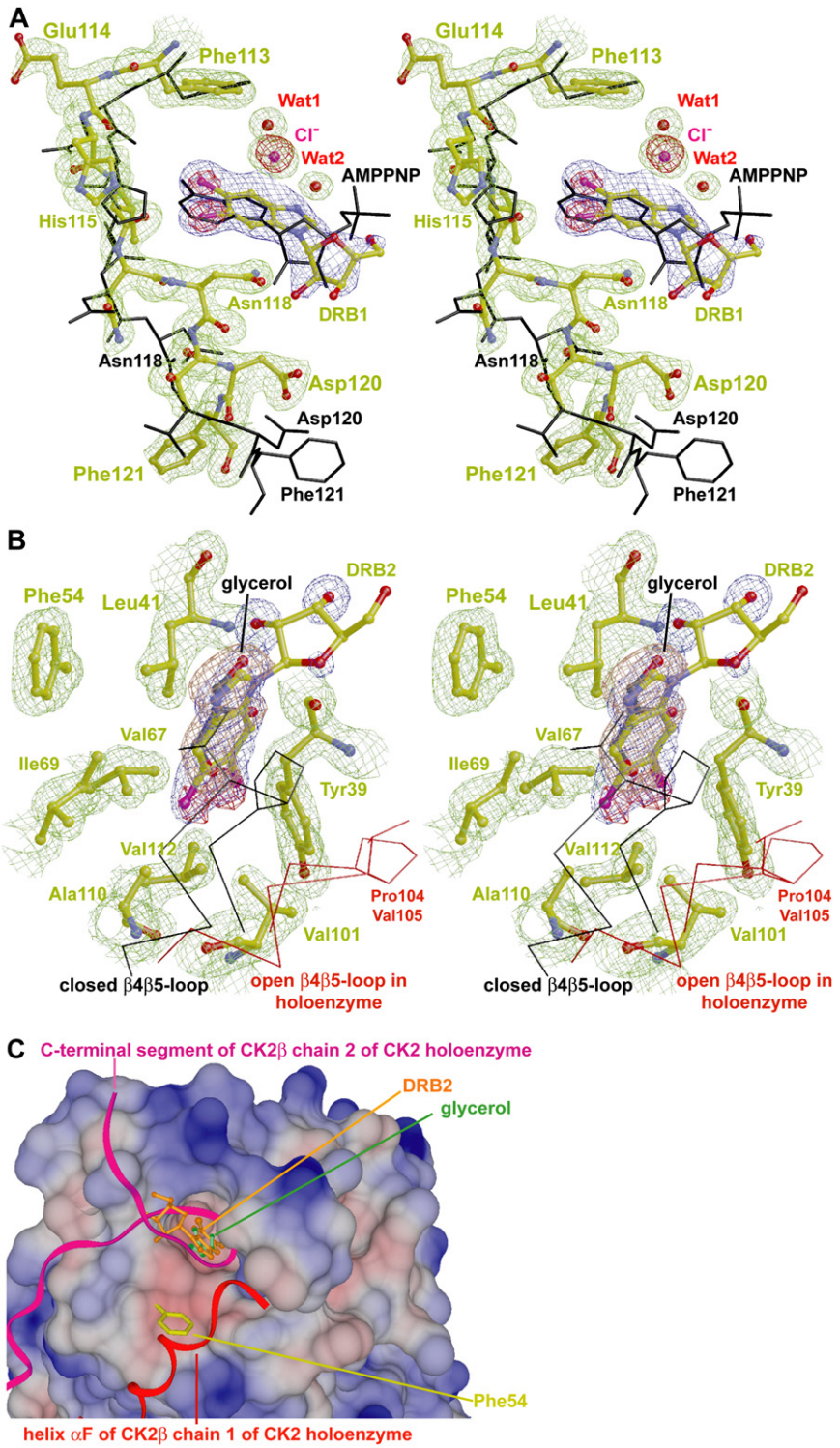


**Figure 2. The Two DRB Binding Sites**

(A) Stereo picture (Esnouf, 1997; Merritt and Bacon, 1997) of DRB1 at the ATP site. The *hs*CK2$\alpha^{1-335}$/DRB complex is covered with $2F_o - F_c$ electron density (contour level 1.0 σ) colored either in green (protein, two water molecules, and one chloride ion) or in blue (DRB). A part of the *hs*CK2$\alpha^{1-335}$/AMPPNP complex (Niefind et al., 2007) is drawn as black sticks. The red cages show anomalous Fourier density (contour level 6 σ).

(B) Stereo picture of the allosteric site occupied by either DRB2 (blue $2F_o - F_c$ density) in the *hs*CK2$\alpha^{1-335}$/DRB complex or by glycerol (gray C atoms, orange $2F_o - F_c$ density) in the *hs*CK2$\alpha^{1-335}$/V66A/M163L/glycerol complex. The surrounding hydrophobic side chains (green $2F_o - F_c$ density) stem from the *hs*CK2$\alpha^{1-335}$/DRB complex. All pieces of $2F_o - F_c$ electron density are contoured at 1 σ. The two chloro substituents of DRB are covered by anomalous Fourier density (red cage; contour level 3.5 σ). The β4β5 loop (black $C_\alpha$ trace and bonds) is drawn for comparison, also in its open form (CK2 holoenzyme; red $C_\alpha$ trace and bonds).

(C) Hydrophobicity surface of the allosteric site of the *hs*CK2$\alpha^{1-335}$/DRB complex and its environment drawn with BRAGI (Schomburg and Reichelt, 1988). Blue color, hydrophilic surface; red color, hydrophobic patches. Parts of the CK2β chains in the CK2 holoenzyme (Niefind et al., 2001) were drawn after 3D fit.

with an $F_o - F_c$ omit map (Figure 1) and with an anomalous Fourier map based on an additional diffraction data set collected at a wavelength of 2 Å at which the anomalous dispersion effect of chlorine is increased. In fact, in this map, the chloro substituents of both DRB molecules together with several chloride ions became visible (Figures 2 and 3).

## The ATP-Competitive DRB Site and Its Conformational Plasticity

According to a well-established pharmacophore model of the ATP site of EPKs (Traxler and Furet, 1999), the DRB1 benzimidazole group occupies the "adenine region" yet without forming H bonds to the interdomain hinge. The adjacent hydrophobic region I that is fairly small in CK2α as a result of a large gatekeeper residue (Phe113) is filled with two water molecules and a chloride ion (Figure 2A).

The hydrophobic region II, however, at the outer region of the ATP binding cleft is occupied by the enzyme itself, namely by Asn118 and other parts of the hinge region (Figure 2A). Although not involved in crystalline contacts, this region adopts a "closed" conformation and restricts the space at the ATP binding site. In contrast, it is open and less space demanding in the structure of *hs*CK2$\alpha^{1-335}$ in complex with adenylyl imidodiphosphate (AMPPNP) (Niefind et al., 2007; Figure 2A). A particularly striking flag is Phe121: it points to the surface in the *hs*CK2$\alpha^{1-335}$/AMPPNP structure but is buried in the *hs*CK2$\alpha^{1-335}$/DRB complex.

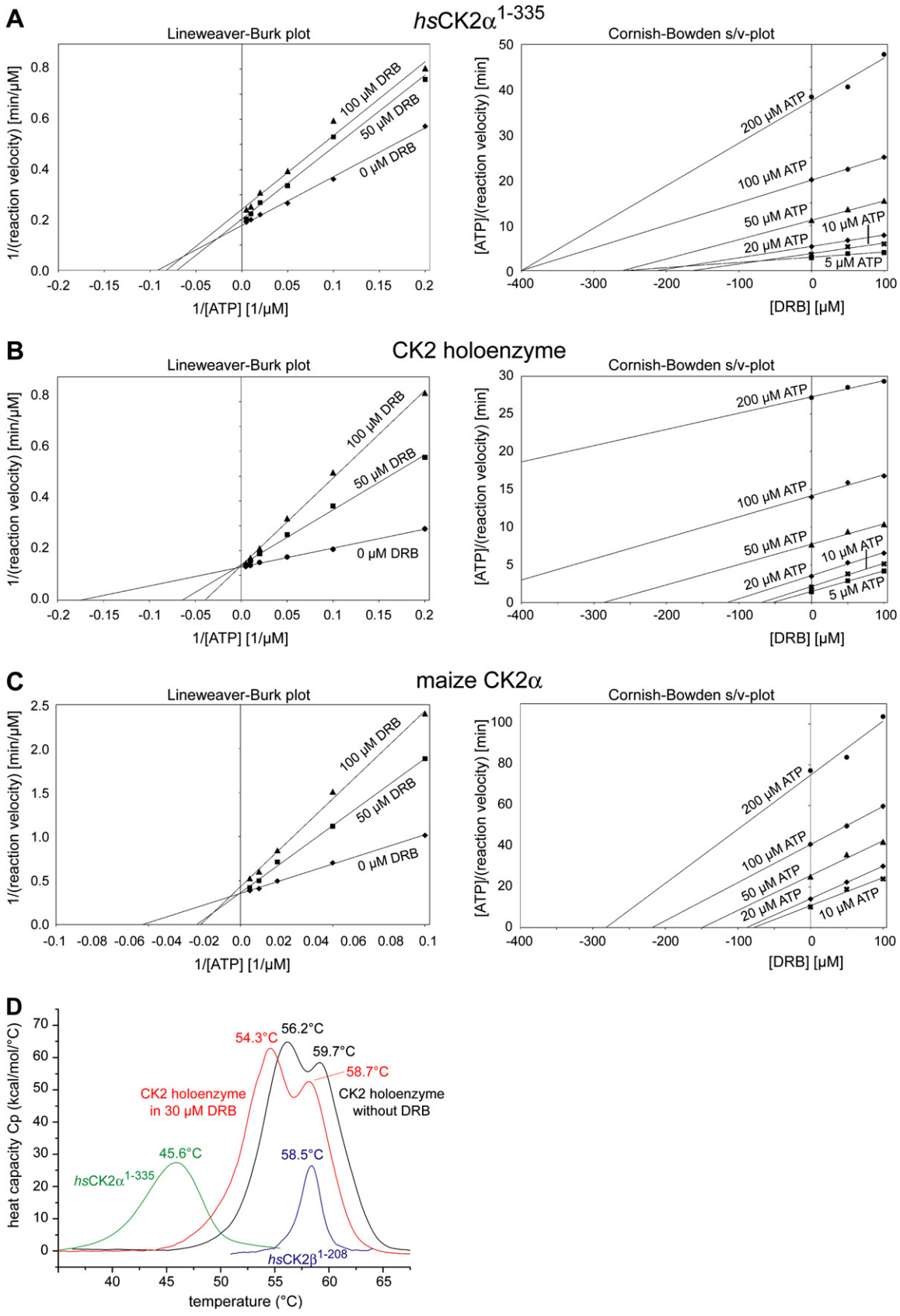
A
hsCK2α1-335
Lineweaver-Burk plot
1/(reaction velocity) [min/μM]
1/[ATP] [1/μM]
100 μM DRB
50 μM DRB
0 μM DRB
Cornish-Bowden s/v-plot
[ATP]/(reaction velocity) [min]
[DRB] [μM]
200 μM ATP
100 μM ATP
50 μM ATP
20 μM ATP
10 μM ATP
5 μM ATP
B
CK2 holoenzyme
Lineweaver-Burk plot
1/(reaction velocity) [min/μM]
1/[ATP] [1/μM]
100 μM DRB
50 μM DRB
0 μM DRB
Cornish-Bowden s/v-plot
[ATP]/(reaction velocity) [min]
[DRB] [μM]
200 μM ATP
100 μM ATP
50 μM ATP
20 μM ATP
10 μM ATP
5 μM ATP
C
maize CK2α
Lineweaver-Burk plot
1/(reaction velocity) [min/μM]
1/[ATP] [1/μM]
100 μM DRB
50 μM DRB
0 μM DRB
Cornish-Bowden s/v-plot
[ATP]/(reaction velocity) [min]
[DRB] [μM]
200 μM ATP
100 μM ATP
50 μM ATP
20 μM ATP
10 μM ATP
D
heat capacity Cp (kcal/mol/°C)
temperature (°C)
54.3°C
56.2°C
59.7°C
58.7°C
CK2 holoenzyme
in 30 μM DRB
CK2 holoenzyme
without DRB
45.6°C
58.5°C
hsCK2α1-335
hsCK2β1-208

To check the unique fold of this region, we performed local similarity searches, submitting the corresponding coordinates (Phe113–Phe121) from either the *hs*CK2α$^{1-335}$/DRB structure (closed conformation) or *hs*CK2α$^{1-335}$/AMPPNP structure (Niefind et al., 2007; open conformation) to the SPASM server (Kleywegt, 1999). We accepted the default parameters except for the atom selection, for which we used the options "CA atoms only" for the initial and "main-chain atoms only" for the finer screening. From the two databases available, we selected the large one (19,094 PDB ID codes). Whereas the open conformation occurred in several EPK structures including those of maize CK2α, the closed conformation provided just a single hit among EPKs, namely the aforementioned mutant *hs*CK2α$^{1-335}$/Val66Ala/Met163Leu (Yde et al., 2005). This particular characteristic of the closed conformation can possibly be exploited to design novel selective type I CK2 inhibitors or to improve the selectivity of existing ones (Nie et al., 2007). Moreover, this specific conformation is not, as assumed earlier (Yde et al., 2005), a consequence of mutations next to the hinge region. Rather, the two distinct local conformations disclose a structural plasticity which seems to be a special feature of human CK2α, as it is not reflected (so far) by the more numerous structures of maize CK2α.

## The Allosteric DRB Site at the Interface to CK2β

In contrast to DRB1, the ribose moiety of DRB2 is partly disordered but the flat benzimidazole group is clearly visible and plugs in a pocket formed by several hydrophobic side chains of the β sheet and the β4β5 loop (Figure 2B). The loop is bent toward the sheet so that its hydrophobic tip residues (Pro104, Val105) participate in the pocket wall.

The β4β5 loop adapts this closed conformation in all structures of monomeric human CK2α published so far (irrespective of the crystal packing or the presence of a ligand). By contrast, it is open in nearly all known structures of maize CK2α and in the human CK2 holoenzyme (Niefind et al., 2001; Figure 2B), where it is involved in the CK2α/CK2β interaction. Hence, DRB2 and a closed β4β5 loop potentially interfere with the docking of CK2β to CK2α. Moreover, the loop provides a further example of a subtle conformational plasticity of CK2α which is evident from the human enzyme but not from the maize homolog.

## Inhibition Kinetic and Calorimetric Studies

The coexistence of an ATP-competitive and an allosteric DRB site should lead to a mixed inhibition of *hs*CK2α$^{1-335}$ by DRB, but to a pure competitive inhibition of the CK2 holoenzyme (unless DRB overcomes the blockade of the allosteric site by CK2β). We confirmed these expectations by kinetic measurements with *hs*CK2α$^{1-335}$ and a CK2 holoenzyme variant (Figures 3A and 3B). For comparison, we included maize CK2α in this analysis. In this case, the inhibition type is predominantly competitive (Figure 3C); however, a certain noncompetitive portion and thus a slight affinity of DRB to an allosteric site is perceptible from the plots.

In a quantitative analysis of the human CK2/CK2α data, we determined a competitive inhibition constant $K_{Ic}$ of 29.2 μM and a noncompetitive constant ($K_{Iu}$) of 39.7 μM. To derive $K_{Iu}$ from the relevant equation describing mixed inhibition, it is necessary to know $K_{Ic}$. Therefore, we first determined $K_{Ic}$ from the measurement with the CK2 holoenzyme (Figure 3B) and then assumed this value (29.2 μM) to be valid also for the ATP-competitive part of the mixed inhibition of *hs*CK2α$^{1-335}$ (Figure 3A).

The $K_{Ic}$ and $K_{Iu}$ values show that the affinity of DRB to the allosteric site is lower than to the ATP site and not sufficient to let DRB efficiently disturb the CK2 holoenzyme architecture. We confirmed by gel-filtration studies (results not illustrated) that DRB can neither induce the dissociation nor prevent the association of the CK2 holoenzyme.

We could, however, detect a subtle impact of DRB on the CK2 holoenzyme architecture by differential scanning calorimetry. The two holoenzyme components stabilize each other by association so that the melting temperature of *hs*CK2α$^{1-335}$ increases from 45.6°C to 56.2°C and that of *hs*CK2β$^{1-208}$ from 58.5°C to 59.7°C (Figure 3D). Yet in the presence of DRB, the melting points of the holoenzyme decrease to 54.3°C and 58.7°C, respectively. We found this effect of DRB to be concentration independent, which is plausible because DRB acts catalytically: it binds to *hs*CK2α$^{1-335}$ and supports the dissociation of the holoenzyme, but afterward at this temperature range *hs*CK2α$^{1-335}$ immediately unfolds so that DRB is released.

## Bioinformatic Surface Analysis

Can DRB thus serve as a starting point to develop an antagonist of the CK2α/CK2β interaction? To assess this question, we submitted the protein part of the *hs*CK2α$^{1-335}$/DRB structure to the Mark-Us server (http://luna.bioc.columbia.edu/honiglab/mark-us/) which includes the SCREEN method (Nayal and Honig, 2006) to identify and characterize surface cavities. Sixteen cavities were detected with the DRB1 site at the top and the DRB2 site at position 3 ranked by the floor surface area ($area_{DRB1\ site}$ = 786 Å$^2$, $area_{DRB2\ site}$ = 113 Å$^2$). In other attributes identified as key criteria for "druggability" (Nayal and Honig, 2006), such as the average depth or maximum depth, the DRB2 site achieved rank 2.

**Figure 3. DRB Effect on Enzymatic Activity and Thermostability**

(A–C) Inhibition kinetic with *hs*CK2α$^{1-335}$ (A), a CK2 holoenzyme construct (B), and maize CK2α (C). Left side: Lineweaver-Burk plots; right side: s/v plots according to Cornish-Bowden (1974). In the case of pure competitive inhibition, the s/v plot shows parallel lines like in (B).

(D) Differential scanning calorimetry (DSC) with *hs*CK2α$^{1-335}$ (green), *hs*CK2β$^{1-208}$ (blue), and the holoenzyme complex both without DRB (black) and in the presence of 30 μM DRB (red). The holoenzyme had the composition (*hs*CK2α$^{1-335}$)$_2$(*hs*CK2β$^{1-208}$)$_2$. The proteins were prepared as described by Niefind et al. (2001, 2007) and Boldyreff et al. (1993). The enzymatic activity was determined at 37°C with a coupled assay containing 100 mM Tris/HCl (pH 8.3), 20 mM $MgCl_2$, 1 mM phosphoenolpyruvate, 3 mg/ml casein, 5 μg/ml lactate dehydrogenase, 5 μg/ml pyruvate kinase, 0.2 mM NADH, and either 0.02 mg/ml *hs*CK2α$^{1-335}$ (A), 0.034 mg/ml CK2 holoenzyme (B), or 0.02 mg/ml maize CK2α (C). In the case of the holoenzyme, 200 mM KCl was additionally present. The ATP and DRB concentrations were varied as indicated on the plots. The reaction was observed via NADH absorption at 340 nm. Each data point represents the average of three experiments. The DSC curves (D) were measured with a MicroCal VP-DSC device. Each test solution contained 60 μM protein in 500 mM NaCl, 25 mM Tris/HCl (pH 8.5). To obtain the red curve, 30 μM DRB and 2% dioxane were additionally present. As shown by control runs, dioxane at this concentration did not affect the melting curves. An increase of the DRB concentration to 100 μM had no additional effect on the melting points. For each case, four independent curves were measured. One representative example is drawn, but the melting points given in (D) are averages over all four experiments.

SCREEN assigned 11 residues to the DRB2 cavity. Some of them (Gln36, Asp37, Asp103, Val112) do not touch the DRB2 ligand, that is, the cavity offers additional interaction possibilities than used by DRB, thus opening a potential for optimization. This conclusion is emphasized by the observation that the list of cavity residues found computationally is not complete: first the DRB2 ligand makes contacts (e.g., Gln40) not listed by SCREEN, and a second visual inspection allows assigning Phe54—a main contact residue to both chains of the CK2β dimer (Niefind et al., 2001; Figure 2C)—and further residues to the allosteric cavity.

Given these limitations of the prediction method, it is encouraging that it computes for the DRB2 pocket the third largest overall "druggability index" among the 16 cavities. With 0.14 (on a scale from 0 to 1), its value looks small relative to that of the DRB1 site (0.90), but compared to a set of 1286 cavities from 99 proteins (Nayal and Honig, 2006), it is among the top 100 and significantly above the noise level. Thus, targeting the DRB2 site by small molecules appears to be a realistic option.

It is noteworthy that the druggability index of the DRB2 binding region drops close to zero if the SCREEN method is applied to either of the CK2α chains of the CK2 holoenzyme (Niefind et al., 2001) in which the β4β5 loop is open. Therefore, to interfere with the CK2α/CK2β interaction, it looks more promising to address CK2α with a closed β4β5 loop—and to stabilize this loop in its CK2 holoenzyme incompatible conformation (Figure 2B)—rather than with an open β4β5 loop as proposed recently (Laudet et al., 2007).

### Glycerol at the Allosteric Site

Irrespective of the strategy, it would be desirable for ligand design to know of further molecules binding to the DRB2 pocket. We discovered such a molecule when we noticed that the *hs*CK2α$^{1-335}$/DRB crystals are isomorphous to those of the mutant *hs*CK2α$^{1-335}$/V66A/M163L (Yde et al., 2005). We therefore reinspected the *hs*CK2α$^{1-335}$/V66A/M163L structure (Table 1) specifically at the allosteric site. In fact, we detected a piece of electron density that fitted perfectly to a glycerol molecule (orange density in Figure 2B). Because *hs*CK2α$^{1-335}$/V66A/M163L had been only temporarily in contact with glycerol during purification, the protein must have captured the ligand and retained it during crystallization (Yde et al., 2005).

Remarkably, the glycerol molecule overlaps largely with DRB2 (Figures 2B and 2C). The specificity of the DRB2 cavity is obviously low, and more chemically diverse ligands might possibly be discovered. Finally, a molecule combining the individual ligand frames might be constructed which is able to compete with CK2β and simultaneously unfold a stronger noncompetitive inhibition effect than DRB.

## SIGNIFICANCE

**A dual binding mode of 5,6-dichloro-1-β-D-ribofuranosyl-benzimidazole (DRB) to the catalytic subunit of human protein kinase CK2 (CK2α) is described. One DRB molecule occupies the canonical ATP cleft. It induces unexpected structural adaptations of the hinge region linking the two main kinase domains that might be pharmacologically important. The second DRB molecule targets the outer surface of the N-terminal β sheet which normally forms the interface to the noncatalytic subunit CK2β. Consistently, we detected with differential scanning calorimetry that DRB disturbs the CK2α/CK2β contact. DRB might therefore serve as a lead structure to develop small-molecule antagonists against the CK2α/CK2β interaction (Wells and McClendon, 2007).**

## ACCESSION NUMBERS

Structures and diffraction data have been deposited in the Protein Data Bank under ID codes 2RKP (*hs*CK2α$^{1-335}$/DRB) and 3BW5 (*hs*CK2α$^{1-335}$/V66A/M163L/glycerol).

## ACKNOWLEDGMENTS

We thank Dr. Manfred Weiss for assistance at the EMBL outstation in Hamburg and the Deutsche Forschungsgemeinschaft (grant NI 643/1-3) and the Forskningsråd for Natur og Univers (grant 272-07-0257) for funding. The authors declare that they have no competing financial interests.

Received: August 24, 2007
Revised: December 24, 2007
Accepted: December 28, 2007
Published: February 22, 2008

## REFERENCES

Boldyreff, B., Meggio, F., Pinna, L.A., and Issinger, O.-G. (1993). Reconstitution of normal and hyperactivated forms of casein kinase-2 by variably mutated β-subunits. Biochemistry *32*, 12672–12677.

CCP4 (Collaborative Computational Project, Number 4) (1994). The CCP4 suite: programs for protein crystallography. Acta Crystallogr. D Biol. Crystallogr. *50*, 760–763.

Cornish-Bowden, A. (1974). A simple graphical method for determining the inhibition constants of mixed, uncompetitive and non-competitive inhibitors. Biochem. J. *137*, 143–144.

Esnouf, R.M. (1997). An extensively modified version of MolScript that includes greatly enhanced coloring capabilities. J. Mol. Graph. Model. *15*, 132–134.

Guerra, B., and Issinger, O.-G. (1999). Protein kinase CK2 and its role in cellular proliferation, development and pathology. Electrophoresis *20*, 391–408.

Huse, M., and Kuriyan, J. (2002). The conformational plasticity of protein kinases. Cell *109*, 275–282.

Kleywegt, G.J. (1999). Recognition of spatial motifs in protein structures. J. Mol. Biol. *285*, 1887–1897.

Knight, Z.A., and Shokat, K.M. (2005). Features of selective kinase inhibitors. Chem. Biol. *12*, 621–637.

Laudet, B., Barrette, C., Dulery, V., Renaudet, O., Dumy, P., Metz, A., Prudent, R., Deshire, A., Dideberg, O., Filhol, O., et al. (2007). Structure-based design of small peptide inhibitors of protein kinase CK2 subunit interaction. Biochem. J. *408*, 363–373.

Manning, G., Whyte, D.B., Martinez, R., Hunter, T., and Sudarsanam, S. (2002). The protein kinase complement of the human genome. Science *298*, 1912–1934.

Meggio, F., Shugar, D., and Pinna, L.A. (1990). Ribofuranosyl-benzimidazole derivatives as inhibitors of casein kinase-2 and casein kinase-1. Eur. J. Biochem. *187*, 89–94.

Merritt, E.A., and Bacon, D.J. (1997). Raster3D: photorealistic molecular graphics. Methods Enzymol. *277*, 505–524.

Nayal, M., and Honig, B. (2006). On the nature of cavities on protein surfaces: application to the identification of drug-binding sites. Proteins *63*, 892–906.

Nie, Z., Perretta, C., Erickson, P., Margosiak, S., Almassy, R., Lu, J., Averill, A., Yager, K.M., and Chu, S. (2007). Structure-based design, synthesis, and study of pyrazolo[1,5-a][1,3,5]triazine derivatives as potent inhibitors of protein kinase CK2. Bioorg. Med. Chem. Lett. *17*, 4191–4195.

 

Niefind, K., Guerra, B., Ermakova, I., and Issinger, O.-G. (2001). Crystal structure of human protein kinase CK2: insights into basic properties of the CK2 holoenzyme. EMBO J. *20*, 5320–5331.

Niefind, K., Yde, C.W., Ermakova, I., and Issinger, O.-G. (2007). Evolved to be active: sulfate ions define substrate recognition sites of CK2α and emphasise its exceptional role within the CMGC family of eukaryotic protein kinases. J. Mol. Biol. *370*, 427–438.

Otwinowski, Z., and Minor, W. (1997). Processing of X-ray diffraction data collected in oscillation mode. Methods Enzymol. *276*, 307–326.

Schomburg, D., and Reichelt, J. (1988). BRAGI: a comprehensive protein modeling program system. J. Mol. Graph. *6*, 161–165.

Seldin, D.C., and Leder, P. (1995). Casein kinase IIα transgene-induced murine lymphoma: relation to theileriosis in cattle. Science *267*, 894–897.

Traxler, P., and Furet, P. (1999). Strategies toward the design of novel and selective protein tyrosine kinase inhibitors. Pharmacol. Ther. *82*, 195–206.

Wells, J.A., and McClendon, C.L. (2007). Reaching for high-hanging fruit in drug discovery at protein-protein interfaces. Nature *450*, 1001–1009.

Yde, C.W., Ermakova, I., Issinger, O.-G., and Niefind, K. (2005). Inclining the purine base binding plane in protein kinase CK2 by exchanging the flanking side-chains generates a preference for ATP as a cosubstrate. J. Mol. Biol. *347*, 399–414.

  